

# We are IntechOpen, the world's leading publisher of Open Access books Built by scientists, for scientists

**4,800**

Open access books available

**122,000**

International authors and editors

**135M**

Downloads

Our authors are among the

**154**

Countries delivered to

**TOP 1%**

most cited scientists

**12.2%**

Contributors from top 500 universities



**WEB OF SCIENCE™**

Selection of our books indexed in the Book Citation Index  
in Web of Science™ Core Collection (BKCI)

Interested in publishing with us?  
Contact [book.department@intechopen.com](mailto:book.department@intechopen.com)

Numbers displayed above are based on latest data collected.

For more information visit [www.intechopen.com](http://www.intechopen.com)



# Dual-Band Resonator Designs for Near-Field Wireless Energy Transfer Applications

*Lai Ly Pon, Mohamed Himdi,  
Sharul Kamal Abdul Rahim and Chee Yen Leow*

## Abstract

Dual-band near-field wireless energy transfer (WET) designs outweigh single-band system with regard to either concurrent energy and data transfer or multiple wireless charging standard functionalities. There are two major approaches in resonator designs, namely, multi-coil and single-coil. This chapter presents a review on design constraints for each design approach and rectification techniques available in counteracting impediments of dual-band near-field WET systems. Challenges pertinent to link design are discussed primarily followed by methods implemented to mitigate detrimental impact on performance metrics. Front-end dual-band resonator design methods are accentuated in this chapter in lieu of end-to-end WET system. This is envisioned to offer insights for designers contemplating on design modes or developing ways to facilitate a boost in rectification options currently available.

**Keywords:** near-field, dual-band, wireless energy transfer, single-coil, multi-coil

## 1. Introduction

The concept of electrical energy propagation with physical interconnection eradication spearheaded by Nikola Tesla has been adapted into diverse low- and high-power wireless energy transfer (WET) applications ranging from wireless charging for consumer electronics to electric vehicles. The massive landscape of consumer electronics has expanded toward healthcare, wellness, and fitness apart from the indispensable smartphones that have become such an integral part of one's daily life. Enhancement on quality of life reaches beyond patients who are dependent on implanted medical devices with healthcare monitoring devices for elderly and disabled communities. Keeping track with one's physical location, activity, and fitness regime is empowered by smart wearables [1]. However, data accumulated from monitoring of heart pacing or metabolic activities require appropriate transmission for further analysis or backup and storage. As such, simultaneous power and data transfer without any physical interconnections such as cables turn out to be an alternative option made possible with the forthcoming fifth generation (5G) technology. Ubiquitous integration of hardware compatibility to support wireless charging for all smart devices is foreseeable.

Provision of more than one frequency band is enabled by resonator which is intended for several functions either concurrent power and data transfer or concurrent wireless charging at multiple standards. At present, there are two principal standards for wireless charging of consumer electronics specifically smartphones. The Wireless Power Consortium, otherwise known as Qi, is one of the leading wireless charging standards operating in low-frequency (LF) band, 110–205 kHz [2]. AirFuel Alliance is the merger between Power Matters Alliance (PMA) and the Alliance for Wireless Power (A4WP, also known as Rezence) [3]. A4WP employs magnetic resonance coupling technique operating at  $6.78 \text{ MHz} \pm 15 \text{ kHz}$  [4], while both Qi and PMA engage in inductive charging technique. The range of PMA's operating frequency is from 277 to 357 kHz [5]. Nonetheless, unlicensed industrial, scientific and medical (ISM) radio bands of up to 13.56 MHz are commonly selected to be the operating frequency for both inductive and magnetic resonant techniques in the current research community [6].

This chapter commences with challenges in relation to dual-band near-field WET design and the corresponding key performance metrics followed by design approaches and rectification techniques currently employed to alleviate the adverse effects on performance metrics with the intention of providing insights for designers in deciding and further enhancing current rectification options available in the design of dual-band near-field resonators. This framework, however, solely pertains to front-end resonator designs excluding end-to-end scope of near-field WET systems.

## 2. Impediments of dual-band near-field wireless energy transfer resonator designs

For a single-band near-field WET resonator design, designers delve into achieving maximum power transfer efficiency (PTE) between a pair of coupled resonators by designing the highest possible quality factor ( $Q$ -factor). However, there is an apparent complexity for designing resonators operating in more than one frequency band. PTE for either one of the frequency bands tends to surpass its counterpart. As such, concurrent capitalization on PTE for both frequency bands,  $f_1$  and  $f_2$ , remains as one of the ultimate challenges.

Another concern is the inversely proportionate relation between  $Q$ -factor and bandwidth. Increasing PTE of the affected frequency band is feasible by developing resonators with enhanced  $Q$ -factor. This comes at the expense of higher bandwidth which is pivotal especially for resonators aiming for concomitant power and data transfer functionalities as portrayed in **Figure 1**. PTE for  $f_1$  is higher with improved  $Q$ -factor than  $f_2$  but falls behind in terms of bandwidth since it is constrained by  $Q$ -factor. On the other hand, redesigning higher  $Q$ -factor resonator in contemplation of attaining improved PTE at  $f_2$  unfortunately leads to bandwidth degradation. As such, there is always a dilemma between achieving PTE equilibrium for  $f_1$  and  $f_2$  and maximum PTE and bandwidth for each frequency bands.

Imperfect positioning of loop resonator is yet another impairment of WET system which impacts its performance metrics specifically coupling coefficient,  $k$ , and PTE [7–9]. Strict adherence toward perfect alignment between a pair of loop resonator in assuring maximum transfer efficiency is seemingly impossible in practical sense because of misalignment be it planar, lateral, or angular frequently supervened [10]. Referring to **Figure 2**, planar displacement refers to the angle of rotation  $\alpha$  when both centers are axially aligned. Separated at a fixed axial distance,  $z$ , the center of receiving loop resonators is shifted by a distance,  $\alpha x$ , known as

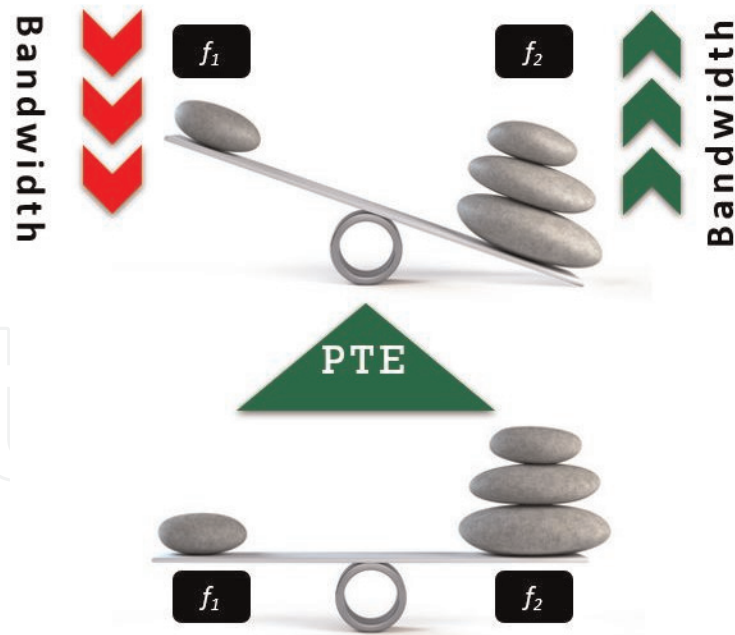


**Figure 1.**  
 Transfer efficiency equilibrium for dual-band near-field coupled resonators.

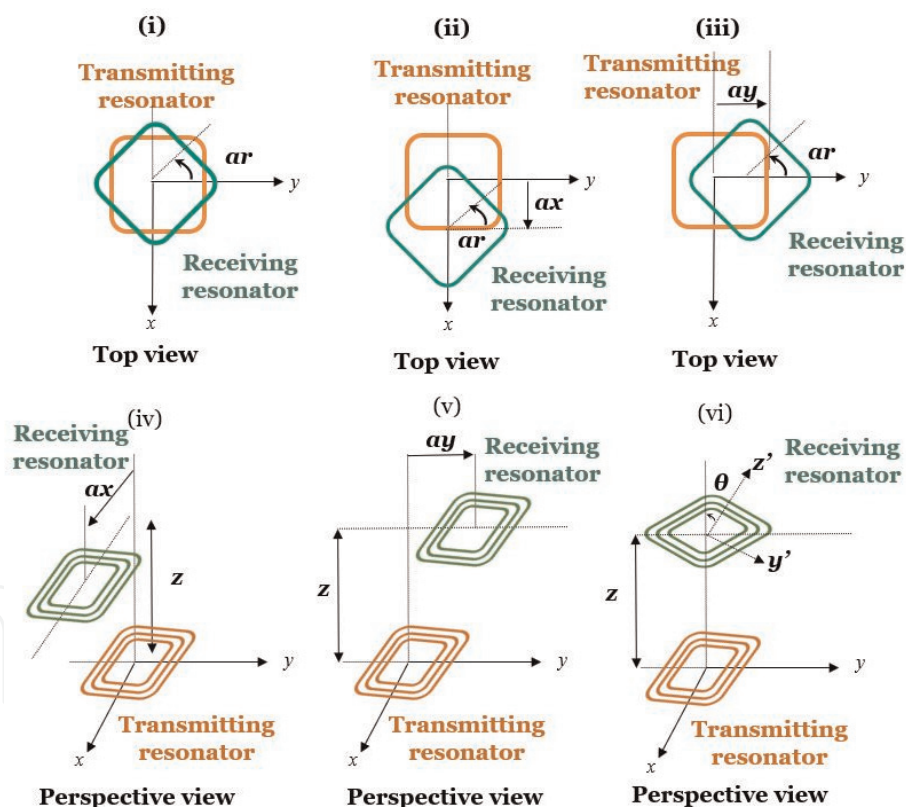


**Figure 2.**  
 Types of displacements between near-field coupled resonators: (i) planar; (ii) concurrent planar and lateral (x-axis); (iii) concurrent planar and lateral (y-axis); (iv) lateral (x-axis), (v) lateral (y-axis); (vi) angular.

horizontal lateral displacement, while  $ay$  is referred as vertical lateral displacement. The occurrence of simultaneous planar and the respective lateral displacements are visualized by  $ar$  with either  $ax$  or  $ay$  offsets. Angular displacement occurs when the plane of receiving loop resonator is being tilted by an angle  $\theta$  [11]. Similarly, the consequences of displacement should be taken into consideration in the design of dual-band coupled resonators.

### 3. Performance metrics

Figure-of-merit (FOM) consideration yields a comparative insight for a diverse WET system design [12]. Derivation of FOM originates from analytical expression of link transfer efficiency (PTE) based on circuit theory (CT) [13] and reflected load theory (RLT) [14] as shown in Eq. (1) and Eq. (2). FOM is reliant on coupling coefficient,  $k$ , and  $Q$ -factor parameters which are derived from Eq. (3) and Eq. (4). Proportional relationship is shared between coupling coefficient,  $k$ , and mutual inductance,  $M$ , with an inverse correlation shared between the latter and product of square root of transmitting and receiving self-inductances,  $L_{1,2}$ .  $Q$ -factor,  $Q_{1,2}$ , is proportional to angular frequency,  $\omega$ , and self-inductances but inversely proportional to transmitting and receiving resistances,  $R_{1,2}$ :

$$PTE = FOM \left[ \left\{ 1 + (1 + FOM)^{0.5} \right\} \right]^{-1} \quad (1)$$

$$FOM = k^2 Q_1 Q_2 \quad (2)$$

$$k = M(L_1 L_2)^{-0.5} \quad (3)$$

$$Q_{1,2} = \omega L_{1,2} (R_{1,2})^{-1} \quad (4)$$

Performance metrics that are commonly used are power transfer efficiency,  $Q$ -factor, and coupling coefficient. As discussed in Section 2, PTE and  $Q$ -factor share a positive correlation which is further validated from Eq. (1) and Eq. (2). Nevertheless, optimum coupling coefficient is often desirable in maximizing PTE. Since  $k$  is dependent on  $M$  and  $M$  is negatively correlated to transfer distance,  $z$ , a cautionary reminder is to ensure optimum transfer distance between transmitting and receiving resonators. This is validated with subsequent Equations [15] that reveal the correlation between  $M$ ,  $z$ , and  $k$  [16].  $M_{ij}$  indicates partial mutual inductance

FOM	Concerned parameters	Dual-band	Significance
$k^2 Q_1 Q_2$	Coupling coefficient, $Q$ -factor transmitting, receiving resonator [12]	No	Independent optimization of $k$ and $Q$ parameters
$PTE^2 P_L (V_s)^{-2}$	Transfer efficiency, load power, and voltage source [17]	No	Take into account of transfer efficiency and power delivered to load
$PTE z^3 (A_{RX})^{-1.5}$	Transfer efficiency, transfer distance, and area of receiver [18, 19]	No	Equitable assessment between various transfer distance and geometry designs
$PTE z (d_o)^{-1}$	Transfer efficiency, transfer distance, and outermost side length [20]	No	Take into account of transfer distance and outermost side lengths
$PTE z (A)^{-0.5}$	Transfer efficiency, transfer distance, and area [21]	No	Equitable assessment between various transfer distance and geometry designs
$PTE z / (d_{o\_tx} \times d_{o\_rx})^{0.5}$	Transfer efficiency, transfer distance, and outermost side lengths of transmitter and receiver [22]	No	Equitable assessment between various transfer distance and asymmetrical pair of resonators
$PTE z (A)^{-0.5}$	Transfer efficiency, transfer distance, and area [23, 24]	Yes	Equitable assessment between various transfer distance and geometry designs

**Table 1.**  
Figure-of-merits (FOM).

between each two turns on a pair of loops with turn radii,  $r_i$  and  $r_j$ .  $\mu$  and  $n_{1,2}$  represent conductor permeability and number of loops' turns, while  $\rho$  is the factor which is dependent on loop profile. K and E refer to complete elliptic integrals of the first and second kind:

$$M_{ij} = 2\mu(r_i r_j)^{0.5} \rho^{-1} [(1 - 0.5\rho^2)K(\rho) - E(\rho)] \quad (5)$$

$$\rho = 2(r_i r_j)^{0.5} [(r_i + r_j)^2 + z^2]^{-0.5} \quad (6)$$

$$M = \rho \sum_{i=1}^{n_1} \sum_{j=1}^{n_2} M_{ij}(r_i, r_j, z) \quad (7)$$

Other FOMs used as performance quantification are summarized in **Table 1**.

#### 4. Frequency selection

There are accompanying implications with the choice of operating frequency on WET links. With higher frequency, the manifestation of eddy currents results in a nonuniformly distributed current density in conductive trace. The probability of current flowing toward the surface of a conductor known as skin effect amplifies alternate current resistance followed by power and heat dissipations [25]. Proximity effect is yet another dilemma of nonuniform current distribution due to current crowding on the inner loop edge caused by nearby conductive traces or layers [26]. On the contrary, current density is uniformly distributed at lower frequency in which eddy current effects are negligible. As such, feasibility of achieving higher power transfer efficiency is established with lower operating frequency at kHz than higher operating frequency at MHz at the expense of transfer range extension and reduced displacement sensitivity [27].

For dual-band WET links, the ratio between frequencies selected is equally important since it is proportional to the transfer efficiency variance between  $f_1$  and  $f_2$  [28]. Additionally, selecting a larger ratio between frequencies with both power and data being transmitted at significantly lower and higher operating frequency bands turns out to be one of the isolation options available in curbing interference [23]. **Table 2** summarizes frequency selections opted for dual-band resonator designs. For example, variance of PTE between kHz and MHz frequencies is larger

References	$f_1$	$f_2$	Ratio, $f_2/f_1$	Variance, $\Delta PTE_{f_1, f_2}$ (%)
[30]	100 kHz	13.56 MHz	136	<10
[29]	100 kHz	6.78 MHz	68	3
[31, 32]	200 kHz	6.78 MHz	34	7.4, <8
[33]	300 MHz	900 MHz	3	8
[24]	300 MHz	675 MHz	2	7
[34–36]	6.78 MHz	13.56 MHz	2	15, 11.93, 1.68
[37]	90.3 MHz	138.8 MHz	2	1
[23]	300 MHz	700 MHz	2	1
[38]	470 MHz	730 MHz	2	11.4

**Table 2.**  
 Summary of frequency selections for dual-band near-field WET resonator.

than MHz frequencies with reduced ratio of  $f_2$  to  $f_1$ . However, research work demonstrated in [29] reports on reduced PTE variance with higher frequency ratio by implementing other rectification techniques which will be discussed in subsequent sections. In general, it is observed that there is higher probability of concurrently capitalizing PTE for both frequencies by designing resonators with lowest possible ratio of  $f_2$  to  $f_1$ .

## 5. Design approaches

Multi-coil [31, 32, 39–42] and single-coil [34, 43, 44] are two predominant strategies in designing dual-band near-field coupled resonators for WET links. Each

Factors	Single-coil	Multi-coil
Cross-coupling	Reduced	More
Geometrical area for resonators	Reduced	More
Concurrent transfer efficiency capitalization for both frequencies	Possible	Increased possibility
Dual-band support configuration	<ul style="list-style-type: none"> <li>• Dual-band TX and dual-band RX resonators</li> <li>• Dual-band TX and single-band RX resonators</li> </ul>	<ul style="list-style-type: none"> <li>• Dual-band TX and dual-band RX resonators</li> <li>• Dual-band TX and single-band RX resonators</li> </ul>

**Table 3.** Comparisons of design approaches for dual-band near-field WET resonator.

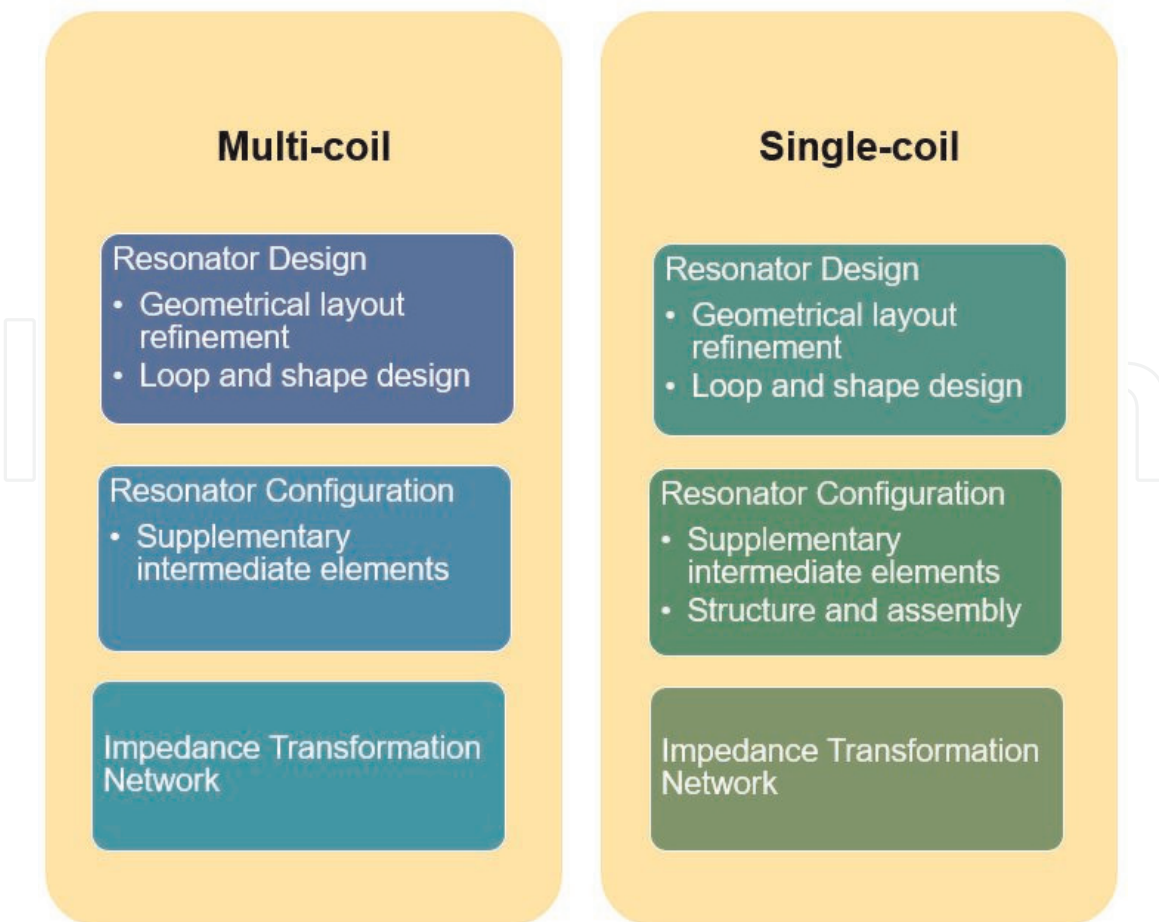


**Figure 3.** Summary of rectification techniques for dual-band near-field WET resonator.

design approach comes with their respective strengths and weaknesses which deserved appropriate assessment as tabulated in **Table 3**. Single-coil approach is preferred owing to minimum cross-coupling as compared to multi-coil [34]. Even though designing two separate coils in multi-coil approach necessitate more geometrical area, there is a greater potential in exploiting on highest possible transfer efficiency at two different frequencies in a single transmitter as it allows independent selection of inductance and quality factor [31].

Apart from deciding on the type of design approach to engage with, dual-band support configuration ought to be determined as well. Applicable configurations [28] involve designing either identical support mode as in dual-band transmitter (TX) and dual-band receiver (RX) or nonidentical support mode as in dual-band transmitter and single-band receivers. Bearing in mind that there is no superior design approach, rectification techniques employed address the respective shortcomings. Referring to **Figure 3**, rectification techniques for dual-band resonator designs which will be discussed in the following subsections encompass aspects relating to resonator design, resonator configuration, and impedance transformation network.

## 6. Rectification techniques

### 6.1 Resonator design

There is a penchant in designing printed spiral coils which encompassed conductive trace etched on dielectric substrates over conventional solenoid coils owing to lightweight and compactness features apart from having privilege of freedom in geometrical optimization [45] and conformity capability on malleable substrates [46] as compared to its predecessor. Equivalent series resistance (ESR) and substrate's dielectric losses are commonly contemplated to boost  $Q$ -factor of loop resonator designed [47] since the performance metric indicator,  $kQ$ , product can be derived from impedance matrix components given by [48]:

$$kQ = |Z_{21}| \text{ESR}^{-1} \quad (8)$$

where  $\text{ESR} = [(R_{11}R_{22}) - (R_{12}R_{21})]^{0.5}$  for two-port system. Despite the fact that higher inductance could be acquired by increasing number of turns, ESR is not exempted. Direct current (DC) and alternate current (AC) resistances are components of ESR for a loop resonator. Hence, it is obligatory to exercise caution in geometrical layout alteration specifically number of turns,  $n$ , conductor width,  $w_c$ , and spacing between conductor trace,  $s_c$ . **Figure 4** illustrates comparison between a conventional layout of spiral resonator with uniform distribution of  $w_c$  and  $s_c$  and nonuniform layout refinement between each loop turns.

By designing inconstant conductor width distributions and spatial distributions,  $Q$ -factor enhancement is attained in double-layer printed spiral resonator [49], printed circular resonator [50], and stacked multilayer printed spiral resonator [51]. This is made possible as losses induced by eddy current are hindered with designs that involve gradual decrement of conductive trace widths from the outermost loop to the innermost loop [52] unlike conventional constant width for all loops. It is worth keeping in mind that designing larger constant conductor width for all turns and smaller constant spacing between adjacent conductor trace will only reinforce the total resistance [53]. However, ensuring ratio between conductor width and spacing to be relatively small aids in the reduction of proximity effects [54].



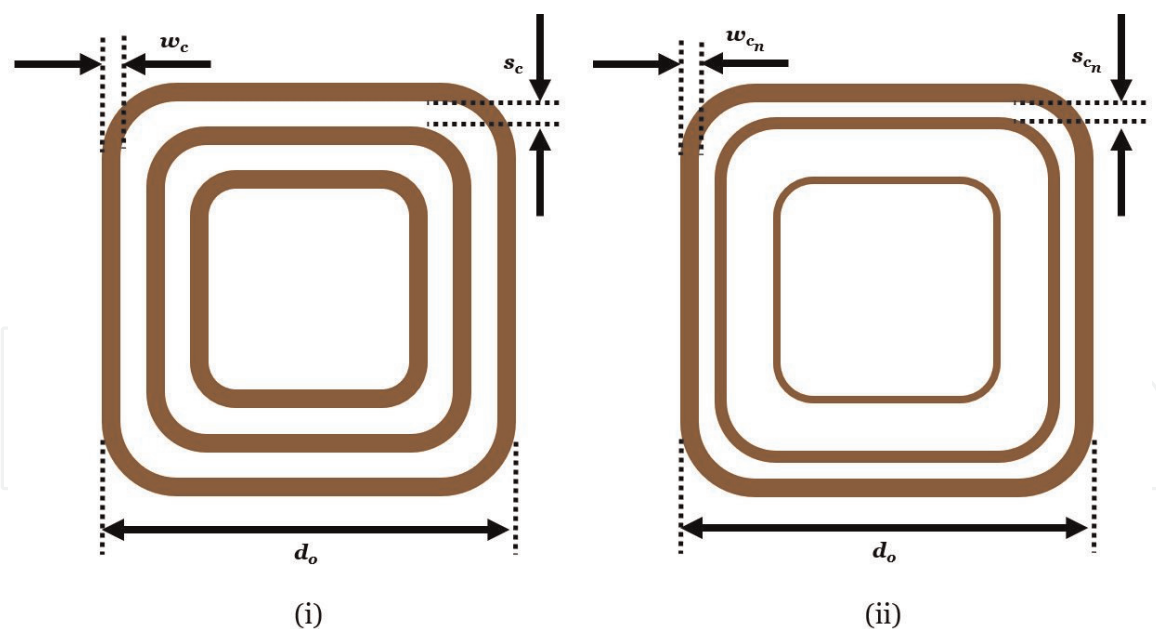


**Figure 4.**  
Geometrical layout refinement: (i) uniform; (ii) nonuniform.

As such, geometrical layout refinement validated in performance enhancement for single-band resonator designs [55–58] can be adopted in resonators designed to operate at more than one frequency band. In [36], multi-coil approach with meticulous geometrical manipulation yields a nonuniform conductor widths and spacing between conductor trace of spiral resonators, collocating in a single-layer substrate. Combined with independent impedance transformation network, which will be covered in ensuing subsection, this leads to minimum transfer efficiency variation between both frequencies.

The prevailing shapes for loop resonator design are circular and square. Nevertheless, there is an upsurge research trend in venturing into other types of resonators with diverse and irregular shapes such as defected ground structure (DGS). DGS resonator designs offer yet another miniaturization technique without forgoing WET performance especially high  $Q$ -factor such as circular DGS [23], interlaced DGS [24], C-shaped DGS [33], and bow-tie DGS [38]. However, the lowest frequency for all these designs hitherto is 300 MHz with ratio between frequency bands of not more than 3.

## 6.2 Resonator configuration

Transfer range deficiency associated with conventional two elements of single-band WET system architecture steers toward the adoption of supplementary elements such as the inclusion of repeaters or relay resonators in between source and load as depicted in **Figure 5**. Hence, sequence of four-coil strongly coupled magnetic resonance (SCMR) configuration introduced in [59], namely, driver, primary, secondary, and load coils, demonstrates extended transfer distance of greater than threefold compared to the diameter of primary resonator. Generally, identical designs can be observed from the driver and load resonators aside from primary and secondary resonators for conventional SCMR configuration. Incorporating repeater as a third element rather than four-element configuration substantiates viability of transfer range extension in single-band WET system [60].

Likewise, incorporating intermediate elements such as repeater in a single-coil approach is a remedy to the predicament in achieving simultaneous high-energy transfer for dual-band as demonstrated in [28, 61]. It is worth noting that additional

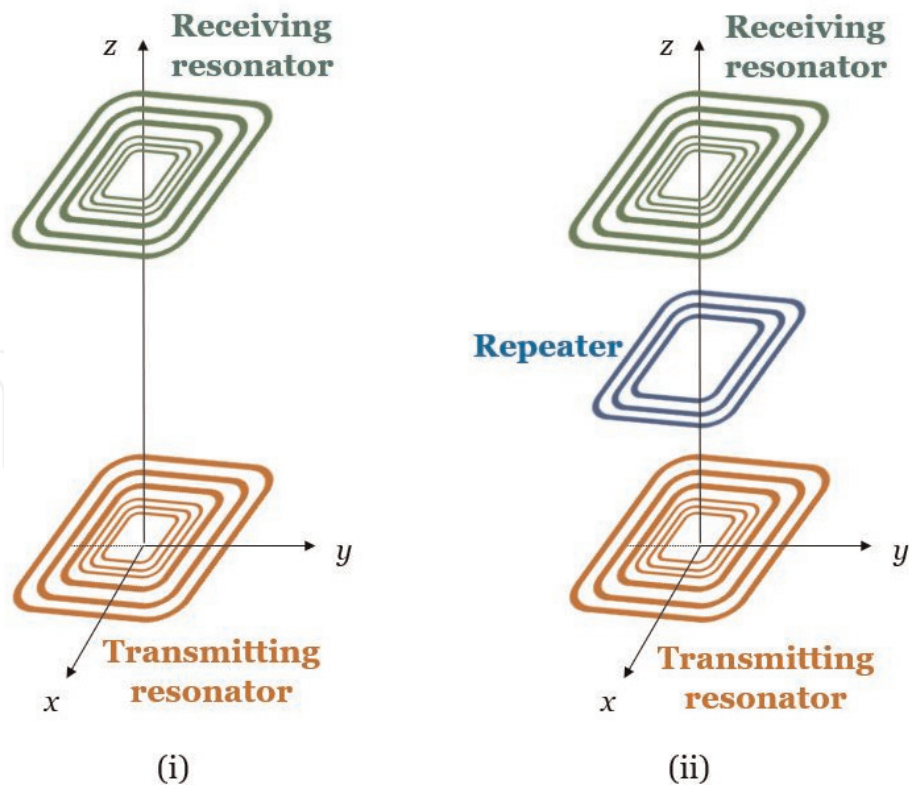


**Figure 5.**  
 Resonator configurations: (i) without intermediate element; (ii) with intermediate element (repeater).

repeater entails more space allocation apart from frequency splitting manifestation of either one of the frequency bands owing to strong coupling. Moreover, designers ought to take into account that transfer efficiency is greatly affected by parasitic resistance originating from repeater.

Composition and construction of resonator is a complementary technique to geometrical layout modification as well as loop and shape design. In multi-coil approach, each resonator operating at  $f_1$  and  $f_2$  can be designed either sharing similar axis or surface as illustrated in **Figure 6** (i) and (ii). The latter alleviates cross-coupling, but larger geometrical area is deemed necessary [39]. Nevertheless, this can be suppressed by designing a pair of asymmetrical coaxial resonators as shown in **Figure 6** (iii) whereby inductance for transmitting resonator is higher than receiving resonator. It is also inferred that optimizing power transfer foremost reduces interference between power carrier and data telemetry since improved coupling that leads to higher transfer power efficiency counterbalances interference between power and data. Further miniaturization effort is described in [24] by

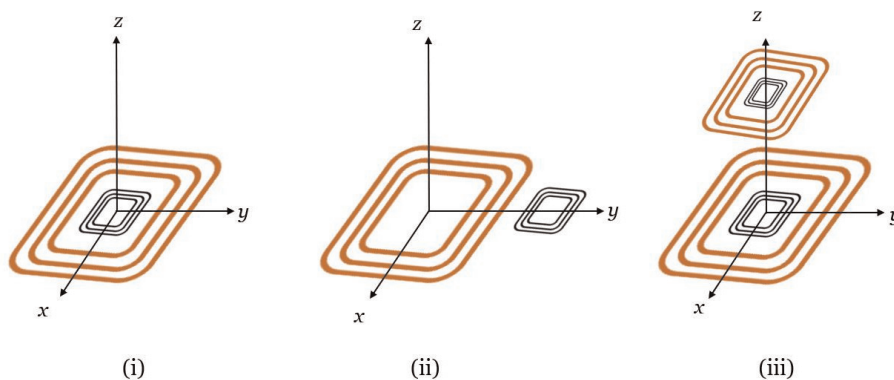


**Figure 6.**  
 Resonator configurations: (i) coaxial; (ii) coplanar; (iii) asymmetrical configuration.

designing a superimposed dual-band DGS instead of coplanar or coaxial configurations.

Furthermore, isolation techniques such as antiparallel loop structure [42] and frequency selective loop [40] structure functioning as band-pass filter have proven effective in rectifying interference caused by multi-coil mode. Band-stop filter in [31] filters' undesired parasitic eddy current from higher frequency induced across lower frequency coil path. The design is then revised in [32] with minimization of large spacing between low and high frequency coils and discrete inductor size along with total number of inverters. With careful combination of impedance values and coil-winding track, magnitude and phase of higher frequency voltage are fine-tuned to attain nil summation of total voltage across lower frequency path. As for displacement countermeasure, constructing more than one loop in an array structure reinforces tolerance toward detrimental consequences caused by imperfect orientations between transmitting and receiving resonators [62]. Robustness toward lateral displacement with wider coverage area is validated in [31] by incorporating asymmetrical configuration technique between a pair of coupled resonators.

### 6.3 Impedance transformation network

Impedance transformation network functions as alleviative measures of mutual inductance disparities triggered by spatial distance or load fluctuations between near-field coupled resonators. Resonance tuning and impedance matching, also referred to as compensation network, are commonly applied as front-end resonator design before AC-DC rectification. Implementing appropriate reactive compensation is necessary toward realizing maximum power transfer efficiency at preferred resonance frequency. **Figure 7** illustrates capacitive compensation topologies which can be generally categorized into symmetrical and asymmetrical compensation network (CN) for single-band near-field WET system. Single capacitive compensation commonly employed each at transmitting and receiving resonator sides encompasses series-series (S-S), parallel-parallel (P-P), series-parallel (S-P), and

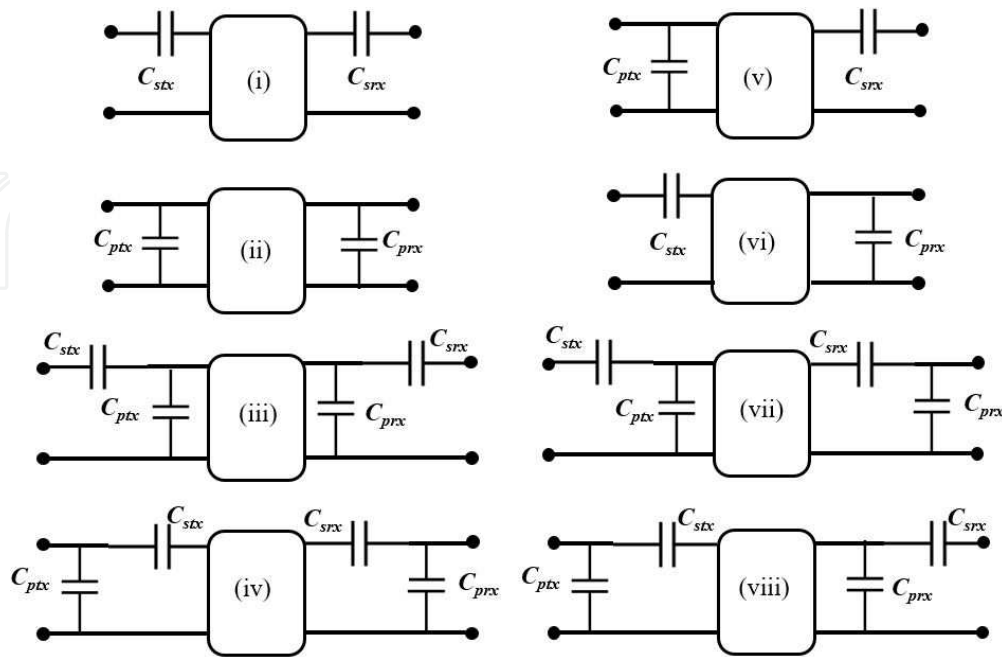


**Figure 7.** Symmetrical compensation network topologies: (i) series-series (S-S); (ii) parallel-parallel (P-P); (iii) series parallel-series parallel (SP-SP); (iv) parallel series-parallel series (PS-PS). Asymmetrical compensation network topologies: (v) parallel-series (P-S); (vi) series-parallel (S-P); (vii) series parallel-parallel series (SP-PS); (viii) parallel series-series parallel (PS-SP).

parallel-series ( $P$ - $S$ ). Double capacitive CN connected either in series or parallel is also known as  $L$ -match network. WET system implemented with complex conjugate matching yields other combination of CN topologies apart from these topologies such as  $T$ -match network [19] as well as hybrid  $T$ -match network of inductor and capacitors [63].

Comprehensive analysis on impedance matching is discussed in [34], which proposes single-coil mode supporting two resonant frequencies at 6.78 and 13.56 MHz thanks to two diverse impedance matching networks comprising of  $LC$  branch in series and  $LC$  tank in parallel. Unfortunately, this method is not applicable when variance between two target frequencies is considerably large particularly if one of the target frequencies originates from kHz band [31]. A way to overcome limitation of vast frequency separation is through specific coil arrangement by positioning inner lower band coil and outer higher band coil [31].

As for multi-coil approach, designers do not have to concern much on the total target frequency separation since impedance matching can be executed independently. In [42], a high and a low  $Q$  impedance matching are performed separately at two different matching distances specifically closer distance for higher transfer efficiency aimed at wireless charging. Conversely, the low  $Q$  impedance match is completed at further distance as a trade-off for higher bandwidth intended for data transfer applications.

Eq. (9) is employed in [36] before performing simultaneous conjugate matching using symmetrical double capacitive CN in order to acquire PTE equilibrium between both frequencies selected. Since the design is based on multi-coil mode, compromise should be made in selecting optimum separation distance between outermost side length of loop operating at  $f_1$  and  $f_2$ . The relationship between optimal transfer distance,  $z_{op\_fn}$ , and outermost side length of loop,  $d_{o\_f1,f2}$ , at maximum excited magnetic field derived in [58] for a square spiral resonator yields:

$$z_{op\_fn} = 0.3931d_{o\_fn} \quad (9)$$

On the other hand, simultaneous high-energy transfer is validated in [23] for both frequency bands using a compact two circular DGS resonators with independent coupling whereby series capacitance is implemented together with single stub for matching method. Correspondingly, comparable findings are also reported in [37] by adopting single-coil approach and single CN with dual-mode printed inductor at a minimized geometrical area requirement. In contrast, DGS resonator designs executed with impedance transformation network which consists of series capacitive lumped element and single stub matching in [24, 38] are unable to acquire minimum PTE variance between frequencies, but these designs excel in terms of maximizing FOM.

## 7. Simulation of dual-band resonator design with multiple rectification techniques

By applying single-coil approach, **Figure 8** depicts an example of dual-band printed spiral resonator simulated with full-wave electromagnetic simulator, CST Microwave Studio separated at transfer distance of 15 mm. Three rectification techniques are implemented specifically resonator design, resonator configuration, and impedance transformation network. Since dimension constrictions are of paramount concern in near-field WET system, the overall dimension of transmitting resonator is limited to 75 mm by 82.5 mm. Other parameter properties are detailed in **Table 4** after optimization of parametric studies via geometrical layout tuning.

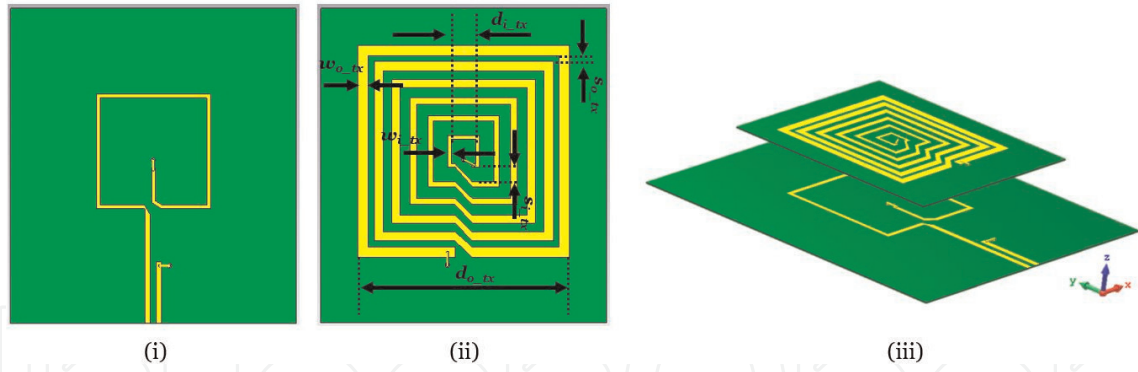


**Figure 8.** Dual-band printed spiral resonator design adopting single-coil approach: (i) transmitter's top layer; (ii) transmitter's bottom layer; (iii) 3D model of transmitting and receiving resonators.

Parameters	Value (mm)
Substrate thickness, $T_s$	0.4
Conductor thickness, $t_c$	0.035
Overall dimension (width $\times$ length)	$75 \times 82.5$
Outermost side length of transmitting resonator, $d_{o\_tx}$	55.8
Innermost side length of transmitting resonator, $d_{i\_tx}$	6.45
Outermost conductor's width of transmitting resonator, $w_{o\_tx}$	2.85
Innermost conductor's width of transmitting resonator, $w_{i\_tx}$	0.98
Outermost conductor's spacing of transmitting resonator, $s_{o\_tx}$	1.5
Innermost conductor's spacing of transmitting resonator, $s_{i\_tx}$	3.75
Size ratio of transmitting to receiving resonators, Tx:Rx	1.5:1

**Table 4.** Parameter properties for dual-band printed spiral resonator design adopting single-coil approach.

Combined with asymmetrical configuration technique, receiving resonator is designed at two-thirds of transmitting resonator's size. Symmetrical hybrid compensation network topology which comprises of inductor and capacitors is incorporated in order to achieve simultaneous conjugate matching at 6.78 and 13.56 MHz as shown in **Figure 9**. LC tank is added with series-parallel capacitive compensation topology for single-coil approach. Values of optimized lumped elements are detailed in **Table 5**. **Figure 10** shows simulated  $S_{11}$  and  $S_{21}$  plots. Despite attaining two distinct resonance frequencies at the intended  $f_1$  and  $f_2$ , feasibility in supporting data transmission at higher frequency is affected as the corresponding  $-3$  dB fractional bandwidth is unfortunately low at approximately 5%. Nevertheless, it is observed that the highest simulated PTE is realized at lower frequency, while

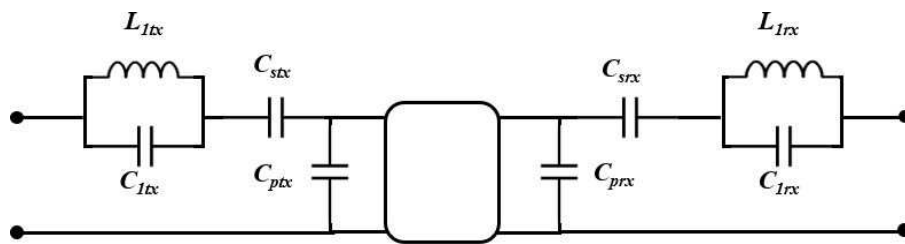


**Figure 9.** Symmetrical hybrid compensation network topology for dual-band printed spiral resonator design adopting single-coil approach.

Parameters	Value
$L_{1tx}$	4.15 $\mu$ H
$C_{1tx}$	8.5 pF
$C_{stx}$	94.65 pF
$C_{ptx}$	184.69 pF
$L_{1rx}$	2.25 $\mu$ H
$C_{1rx}$	4.32 pF
$C_{srx}$	77.58 pF
$C_{prx}$	269.10 pF

**Table 5.** Symmetrical hybrid compensation properties for dual-band printed spiral resonator design adopting single-coil approach.

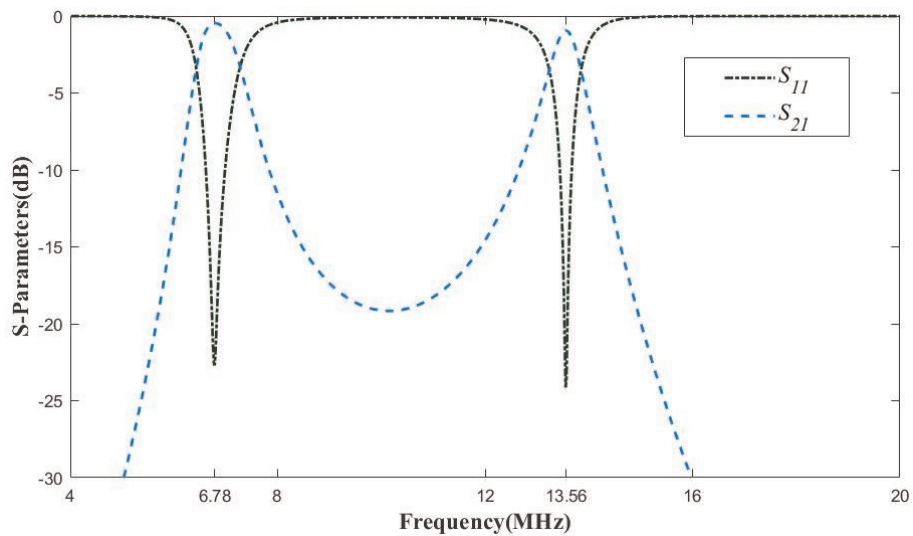


**Figure 10.** Simulated  $S$ -parameter plots of dual-band printed spiral resonator design adopting single-coil approach.

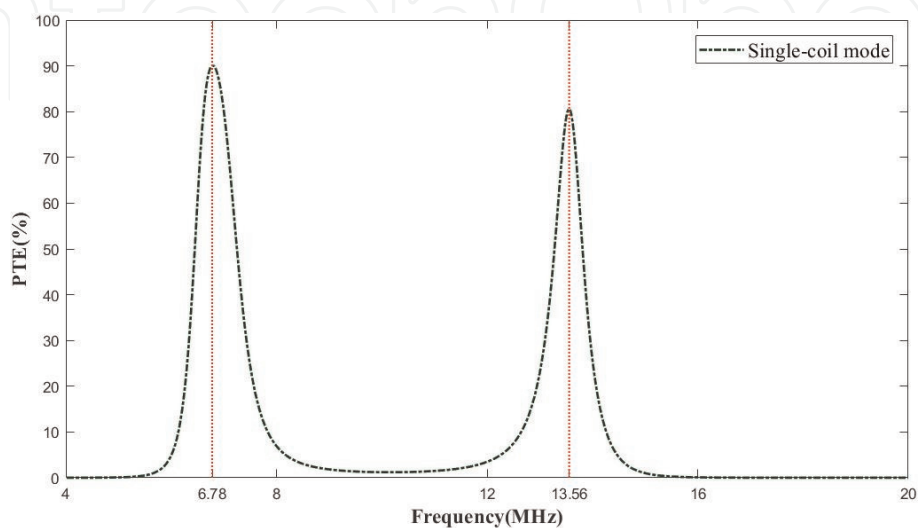


**Figure 11.** Simulated power transfer efficiency plot of dual-band printed spiral resonator design adopting single-coil approach.

minimum variation of PTEs is preserved as depicted in **Figure 11**. Positioned at perfect alignment, PTE for each frequency is 90.11 and 80.56% at 6.78 and 13.56 MHz, respectively. Variation of PTEs at 9.55% is satisfactory considering ratio between frequencies is significantly small at only two for single-coil approach.

## 8. Conclusions

Constraints of dual-band near-field wireless energy transfer links are presented. Front-end mitigation techniques in sustaining acceptable performance metrics for dual-band WET system are reviewed. Accomplishment of satisfactory transfer efficiency at a relevant axial distance regardless of resonance frequencies preferred is imperative besides having resilience against coupling variations and displacement offset from ideal orientation. Deciding on the design approaches conveyed above is narrowed down to either meeting specifications of transfer efficiency proportionality between selected frequencies or sufficient energy and data transfer capability. As such, precautionary steps should be undertaken in determining technique adoption in an effort to strike a balance between performance goals, design complexity, and physical and budgetary restraints. All the aforementioned techniques discussed in this chapter serve as a benchmark or recommended framework for designers' discretion.

## Acknowledgements

This work is jointly supported by CREST under Grant 4B151 and the Institute of Electronics and Telecommunication of Rennes (IETR).

## Conflict of interest

The authors declare no conflict of interest.

## Notes/Thanks/Other declarations

Thanks to Kristina Tijan for invitation to contribute this chapter to the book "Wireless Energy Transfer Technology".

## Appendixes and nomenclature

Symbol	Parameter
$f_{1,2}$	frequency 1, 2
$k$	coupling coefficient
$ar$	planar displacement
$ax$	horizontal lateral displacement
$ay$	vertical lateral displacement
$\theta$	angular displacement
$z$	transfer distance

Symbol	Parameter
$z_{op\_fn}$	optimal transfer distance
$Q_{1,2}$	$Q$ -factor transmitting or receiving resonator
$M$	mutual inductance
$L_{1,2}$	inductance of transmitting or receiving resonator
$P_L$	load power
$V_s$	voltage source
$A_{RX}$	area, area of receiving resonator
$d_{o\_tx, o\_rx}$	outermost side lengths of transmitting or receiving resonator
$d_{i\_tx, i\_rx}$	innermost side length of transmitting or receiving resonator
$n$	turns
$w_c$	conductor's width
$w_{o\_tx}$	outermost conductor's width of transmitting resonator
$w_{i\_tx}$	innermost conductor's width of transmitting resonator
$s_c$	conductor's spacing
$s_{o\_tx}$	outermost conductor's spacing of transmitting resonator
$s_{i\_tx}$	innermost conductor's spacing of transmitting resonator
$T_s$	substrate thickness
$t_c$	conductor thickness
$L_{1tx, 1rx}$	simulated inductor at transmitting or receiving resonator
$C_{1tx, 1rx}$	simulated capacitor at transmitting or receiving resonator
$C_{stx, srx}$	simulated series capacitor at transmitting or receiving resonator
$C_{ptx, prx}$	simulated parallel capacitor at transmitting or receiving resonator

## Author details


Lai Ly Pon<sup>1</sup>, Mohamed Himdi<sup>2\*</sup>, Sharul Kamal Abdul Rahim<sup>1</sup> and Chee Yen Leow<sup>1</sup>

<sup>1</sup> Wireless Communication Center, School of Electrical Engineering, Faculty of Engineering, Universiti Teknologi Malaysia, Johor Bahru, Malaysia

<sup>2</sup> Institute of Electronics and Telecommunication of Rennes, University of Rennes 1, Rennes, France

\*Address all correspondence to: [mohamed.himdi@univ-rennes1.fr](mailto:mohamed.himdi@univ-rennes1.fr)

## IntechOpen

© 2019 The Author(s). Licensee IntechOpen. This chapter is distributed under the terms of the Creative Commons Attribution License (<http://creativecommons.org/licenses/by/3.0/>), which permits unrestricted use, distribution, and reproduction in any medium, provided the original work is properly cited. 



## References

- [1] Piwek L, Ellis DA, Andrews S, Joinson A. The rise of consumer health wearables: Promises and barriers. *PLoS Medicine*. 2016;**13**:1-9. DOI: 10.1371/journal.pmed.1001953
- [2] Wireless Power Consortium. The Qi Wireless Power Transfer System Power Class 0 Specification Parts 1 and 2: Interface Definitions; 2016
- [3] Merger Information. Retrieved from Airfuel website: <http://www.airfuel.org/news/merger-information>, (n.d.)
- [4] Technical Working Committees (TWC 1+2) of the Alliance for Wireless Power (A4WP), A4WP Wireless Power Transfer System Baseline System Specification (BSS) v 1.2.1, A4WP Stand; 2014
- [5] Chandrasekar Rao TS, Geetha K. Categories, standards and recent trends in wireless power transfer: A survey. *Indian Journal of Science and Technology*. 2016;**9**:11. DOI: 10.17485/ijst/2016/v9i20/91041
- [6] Trivedi Y. Wireless power transfer: “Look ma, no hands, no wires! *IEEE Communications Magazine*. 2016;**54**:8. DOI: 10.1109/MCOM.2016.7514157
- [7] Hui SY. Planar wireless charging technology for portable electronic products and qi. *Proceedings of the IEEE*. 2013;**101**:1290-1301. DOI: 10.1109/JPROC.2013.2246531
- [8] Liu D, Hu H, Georgakopoulos SV. Misalignment sensitivity of strongly coupled wireless power transfer systems. *IEEE Transactions on Power Electronics*. 2017;**32**:5509-5519. DOI: 10.1109/TPEL.2016.2605698
- [9] Song M, Belov P, Kapitanova P. Wireless power transfer inspired by the modern trends in electromagnetics. *Applied Physics Reviews*. 2017;**4**:021102. DOI: 10.1063/1.4981396
- [10] Joy ER, Dalal A, Kumar P. Accurate computation of mutual inductance of two air core square coils with lateral and angular misalignments in a flat planar surface. *IEEE Transactions on Magnetics*. 2014;**50**:1-9. DOI: 10.1109/TMAG.2013.2279130
- [11] Flynn BW, Fotopoulou K. Rectifying loose coils: Wireless power transfer in loosely coupled inductive links with lateral and angular misalignment. *IEEE Microwave Magazine*. 2013;**14**:48-54. DOI: 10.1109/MMM.2012.2234634
- [12] Sample AP, Meyer DA, Smith JR. Analysis, experimental results, and range adaptation of magnetically coupled resonators for wireless power transfer. *IEEE Transactions on Industrial Electronics*. 2011;**58**:544-554. DOI: 10.1109/TIE.2010.2046002
- [13] Dionigi M, Mongiardo M, Perfetti R. Rigorous network and full-wave electromagnetic Modeling of wireless power transfer links. *IEEE Transactions on Microwave Theory and Techniques*. 2015;**63**:65-75. DOI: 10.1109/TMTT.2014.2376555
- [14] Kiani M, Ghovanloo M. The circuit theory behind coupled-mode magnetic resonance-based wireless power transmission. *IEEE Transactions on Circuits and Systems I: Regular Papers*. 2012;**59**:2065-2074. DOI: 10.1109/TCSI.2011.2180446
- [15] Jow U, Ghovanloo M. Design and optimization of printed spiral coils for efficient transcutaneous inductive power transmission. *IEEE Transactions on Biomedical Circuits and Systems*. 2007;**1**:193-202. DOI: 10.1109/TBCAS.2007.913130

- [16] Schormans M, Valente V, Demosthenous A. Frequency splitting analysis and compensation method for inductive wireless powering of implantable biosensors. *Sensors (Switzerland)*. 2016;**16**:1229. DOI: 10.3390/s16081229
- [17] Kiani M, Ghovanloo M. A figure-of-merit for designing high-performance inductive power transmission links. *IEEE Transactions on Industrial Electronics*. 2013;**60**:5292-5305. DOI: 10.1109/TIE.2012.2227914
- [18] Zargham M, Gulak PG. Fully integrated on-chip coil in 0.13  $\mu\text{m}$  CMOS for wireless power transfer through biological media. *IEEE Transactions on Biomedical Circuits and Systems*. 2015;**9**:259-271. DOI: 10.1109/TBCAS.2014.2328318
- [19] Yang C, Chang C, Lee S, Chang S, Chiou L. Efficient four-coil wireless power transfer for deep brain stimulation. *IEEE Transactions on Microwave Theory and Techniques*. 2017;**65**:2496-2507. DOI: 10.1109/TMTT.2017.2658560
- [20] Tahar F, Saad R, Barakat A, Pokharel RK. 1.06 FoM and compact wireless power transfer system using rectangular defected ground structure resonators. *IEEE Microwave and Wireless Components Letters*. 2017;**27**:1025-1027. DOI: 10.1109/LMWC.2017.2750032
- [21] Hekal S, Abdel-Rahman AB, Jia H, Allam A, Barakat A, Pokharel RK. A Novel technique for compact size wireless power transfer applications using defected ground structures. *IEEE Transactions on Microwave Theory and Techniques*. 2017;**65**:591-599. DOI: 10.1109/TMTT.2016.2618919
- [22] Liu Z, Chen Z, Li J, Guo Y, Xu B. A planar L-shape transmitter for wireless power transfer system. *IEEE Antennas and Wireless Propagation Letters*. 2016;**1225**:960-963. DOI: 10.1109/LAWP.2016.2615112
- [23] Tahar F, Barakat A, Saad R, Yoshitomi K, Pokharel RK. Dual-band defected ground structures wireless power transfer system with independent external and inter-resonator coupling. *IEEE Transactions on Circuits and Systems II: Express Briefs*. 2017;**64**:1372-1376. DOI: 10.1109/TCSII.2017.2740401
- [24] Sharaf R, Abdel-Rahman AB, El-Hameed ASA, Barakat A, Hekal S, Allam A. A new compact dual-band wireless power transfer system using interlaced resonators. *IEEE Microwave and Wireless Components Letters*. 2019;**49**:498-500. DOI: 10.1109/LMWC.2019.2917747
- [25] Bahl I. *Lumped Elements for RF and Microwave Circuits*. Artech House; 2003
- [26] Kuhn WB, Ibrahim NM. Analysis of current crowding effects in multiturn spiral inductors. *IEEE Transactions on Microwave Theory and Techniques*. 2001;**49**:31-38. DOI: 10.1109/22.899959
- [27] Liu M, Chen M. Dual-band wireless power transfer with reactance steering network and reconfigurable receivers. *IEEE Transactions on Power Electronics*. 2019;**8993**:1-1. DOI: 10.1109/TPEL.2019.2913991
- [28] Kung M-L, Lin K-H. Dual-band coil module with repeaters for diverse wireless power transfer applications. *IEEE Transactions on Microwave Theory and Techniques*. 2018;**66**:332-345. DOI: 10.1109/TMTT.2017.2711010
- [29] Riehl PS, Satyamoorthy A, Akram H, Yen Y-C, Yang J-C, Juan B, et al. *Wireless power Systems for Mobile Devices Supporting Inductive and*

- Resonant Operating Modes. IEEE Transactions on Microwave Theory and Techniques. 2015;**63**:780-790. DOI: 10.1109/TMTT.2015.2398413
- [30] Liu M, Chen M. Dual-band multi-receiver wireless power transfer: Architecture, topology, and control. In: 2019 IEEE Appl. Power Electron. Conf. Expo. New York: IEEE; 2019. pp. 851-859. DOI: 10.1109/APEC.2019.8721837
- [31] Ahn D, Mercier PP. Wireless power transfer with concurrent 200-kHz and 6.78-MHz operation in a single-transmitter device. IEEE Transactions on Power Electronics. 2016;**31**: 5018-5029
- [32] Ahn D, Kim S, Kim S-W, Moon J, Cho I. Wireless power transmitter and receiver supporting 200-kHz and 6.78-MHz dual-band operation without magnetic field canceling. IEEE Transactions on Power Electronics. 2017;**32**:7068-7082. DOI: 10.1109/TPEL.2016.2629494
- [33] Atallah HA, Huseein R, Abdel-Rahman AB. Novel and compact design of capacitively loaded C-shaped DGS resonators for dual band wireless power transfer (DB-WPT) systems. AEÜ - International Journal of Electronics and Communications. 2019;**100**:95-105. DOI: 10.1016/j.aeue.2018.12.016
- [34] Kung ML, Lin KH. Enhanced analysis and design method of dual-band coil module for near-field wireless power transfer systems. IEEE Transactions on Microwave Theory and Techniques. 2015;**63**:821-832. DOI: 10.1109/TMTT.2015.2398415
- [35] Ding K, Yu Y, Lin H. A novel dual-band scheme for magnetic resonant wireless power transfer. Progress In Electromagnetics Research Letters. 2018;**80**:53-59. DOI: 10.258/PIERL18082201
- [36] Pon LL, Kamal S, Rahim A, Leow CY, Chua TH. Non-radiative wireless energy transfer with single layer dual-band printed spiral resonator. Bull. Electr. Eng. Informatics. 2019;**8**:744-752. DOI: 10.11591/eei.v8i3.1593
- [37] Barakat A, Yoshitomi K, Pokharel RK. Design and implementation of dual-mode inductors for dual-band wireless power transfer systems. IEEE Transactions on Circuits and Systems II: Express Briefs. 2018;**66**: 1287-1291. DOI: 10.1109/TCSII.2018.2883671
- [38] Saad MR, Tahar F, Chalise S, Barakat A, Yoshitomi K, Pokharel RK. High FOM dual band wireless power transfer using bow-tie defected ground structure resonators. In: 2018 IEEE Wirel. Power Transf. Conf. New York: IEEE; 2018. pp. 1-4. DOI: 10.1109/WPT.2018.8639134
- [39] Wang G, Wang P, Tang Y, Liu W. Analysis of dual band power and data telemetry for biomedical implants. IEEE Transactions on Biomedical Circuits and Systems. 2012;**6**:208-215. DOI: 10.1109/TBCAS.2011.2171958
- [40] Kwon D, Yeo TD, Oh KS, Yu JW, Lee WS. Dual resonance frequency selective loop of near-field wireless charging and communications systems for portable device. IEEE Microwave and Wireless Components Letters. 2015; **25**:624-626. DOI: 10.1109/LMWC.2015.2451352
- [41] Chung M, Chien Y-L, Cho L, Hsu P, Yang C-F. A dual-mode antenna for wireless charging and near field communication. In: 2015 IEEE Int. Symp. Antennas Propag. Usn. Natl. Radio Sci. Meet. 2015. pp. 1288-1289. DOI: 10.1109/APS.2015.7305033
- [42] Lee W-S, Kim D-Z, Yu J-W. Multi-functional high-isolation dual antenna for controllable wireless charging and

NFC communication. *Electronics Letters*. 2014;**50**:912-913. DOI: 10.1049/el.2014.0858

[43] Dionigi M, Mongiardo M. A novel resonator for simultaneous wireless power transfer and near field magnetic communications. In: *IEEE MTT-S Int. Microw. Symp. Dig.* New York: IEEE; 2012. pp. 8-10. DOI: 10.1109/MWSYM.2012.6259383

[44] Han M, Kim J-M, Sohn H. Dual-mode wireless power transfer module for smartphone application. In: *2015 IEEE Int. Symp. Antennas Propag. Usn. Natl. Radio Sci. Meet.* New York: IEEE; 2015. pp. 111-112. DOI: 10.1109/APS.2015.7304441

[45] Fotopoulou K, Flynn BW. Wireless power transfer in loosely coupled links: Coil misalignment model. *IEEE Transactions on Magnetics*. 2011;**47**: 416-430. DOI: 10.1109/TMAG.2010.2093534

[46] Heo E, Choi K-Y, Kim J, Park J-H, Lee H. A wearable textile antenna for wireless power transfer by magnetic resonance. *Textile Research Journal*. 2018;**88**:913-921. DOI: 10.1177/0040517517690626

[47] Eteng AA, Rahim SKA, Leow CY. Wireless nonradiative energy transfer: Antenna performance enhancement techniques. *IEEE Antennas and Propagation Magazine*. 2015;**57**:16-22. DOI: 10.1109/MAP.2015.2437281

[48] Ohira T. The kQ product as viewed by an analog circuit engineer. *IEEE Circuits and Systems Magazine*. 2017;**17**: 27-32. DOI: 10.1109/MCAS.2016.2642698

[49] Mehri S, Ammari AC, Ben Hadj J, Slama LL. Performance characterization of variable width square coils for inductive link wireless power transfer. In: *2016 18th Mediterr. Electrotech.*

Conf. New York: IEEE; 2016. pp. 1-6. DOI: 10.1109/MELCON.2016.7495447

[50] Kim J, Lee K, Kwon H, Cha C. New structure for high Q-factor printed antenna in wireless power transmission. In: *IEEE EUROCON 2017 -17th Int. Conf. Smart Technol.* New York: IEEE; 2017. pp. 474-478. DOI: 10.1109/EUROCON.2017.8011155

[51] Mehri S, Ammari AC, Slama JBH, Sawan M. Design optimization of multiple-layer PSCs with minimal losses for efficient and robust inductive wireless power transfer. *IEEE Access*. 2018;**6**:31924-31934. DOI: 10.1109/ACCESS.2018.2831785

[52] Hsu H-M. Improving the quality factor of a broadened spiral inductor with arithmetic-progression step width. *Microwave and Optical Technology Letters*. 2005;**45**:118-120. DOI: 10.1002/mop.20741

[53] Klaric Felic G, Ng D, Skafidas E. Investigation of frequency-dependent effects in inductive coils for implantable electronics. *IEEE Transactions on Magnetics*. 2013;**49**:1353-1360. DOI: 10.1109/TMAG.2012.2231091

[54] Mehri S, Ammari AC, Slama J, Sawan M. Minimizing printed spiral coil losses for inductive link wireless power transfer. In: *2016 IEEE Wirel. Power Transf. Conf.* New York: IEEE; 2016. pp. 1-4. DOI: 10.1109/WPT.2016.7498860

[55] Zierhofer CM, Hochmair ES. Geometric approach for coupling enhancement of magnetically coupled coils. *IEEE Transactions on Biomedical Engineering*. 1996;**43**:708-714. DOI: 10.1109/10.503178

[56] Sharma A, Zuazola IJG, Gupta A, Perallos A, Batchelor JC. Non-uniformly distributed-turns coil antenna for enhanced H-field in HF-RFID. *IEEE Transactions on Antennas and*

Propagation. 2013;**61**:4900-4907. DOI: 10.1109/TAP.2013.2275244

[57] Sharma A, Zuazola IJG, Gupta A, Perallos A, Batchelor JC. Enhanced H-field in HF RFID systems by optimizing the loop spacing of antenna coils. *Microwave and Optical Technology Letters*. 2013;**55**:944-948. DOI: 10.1002/mop.27406

[58] Eteng AA, Abdul Rahim SK, Leow CY, Chew BW, Vandenbosch GAE. Two-stage design method for enhanced inductive energy transmission with Q-constrained Planar Square loops. *PLoS One*. 2016;**11**:e0148808. DOI: 10.1371/journal.pone.0148808

[59] Kurs A, Karalis A, Robert M, Joannopoulos JD, Fisher P, Soljacic M. Wireless power transfer via strongly coupled magnetic resonances. *Science* (80-). 2007;**317**:83-86. DOI: 10.1126/science.1143254

[60] Ahn D, Hong S. A study on magnetic field repeater in wireless power transfer. *IEEE Transactions on Industrial Electronics*. 2013;**60**:360-371. DOI: 10.1109/TIE.2012.2188254

[61] Kung M, Lin K. A 6.78 MHz and 13.56 MHz dual-band coil module with a repeater for wireless power transfer systems. In: 2016 IEEE Int. Symp. Antennas Propag. New York: IEEE; 2016. pp. 157-158. DOI: 10.1109/APS.2016.7695787

[62] Lee W-S, Park S, Lee J-H, Tentzeris MM. Longitudinally misalignment-insensitive dual-band wireless power and data transfer systems for a position detection of fast-moving vehicles. *IEEE Transactions on Antennas and Propagation*. 2019;**67**: 5614-5622. DOI: 10.1109/TAP.2019.2916697

[63] Zhu G, Gao D, Wang S, Chen S. Misalignment tolerance improvement in wireless power transfer using LCC

compensation topology. In: 2017 IEEE PELS Work. Emerg. Technol. Wirel. Power Transf. New York: IEEE; 2017. pp. 1-7. DOI: 10.1109/WoW.2017.7959411